Sustainable Energy & Fuels

Mono-Transition-Metal-substituted Polyoxometalates as Shuttle Redox Mediator for Z-scheme Water Splitting under Visible Light

Journal:	*Sustainable Energy & Fuels*
Manuscript ID	SE-ART-10-2021-001619.R1
Article Type:	Paper
Date Submitted by the Author:	22-Nov-2021
Complete List of Authors:	Tomita, Osamu; Kyoto University, Graduate School of Engineering Naito, Hiroki; Kyoto University, Graduate School of Engineering Nakada, Akinobu; Kyoto University, Graduate School of Engineering Higashi, Masanobu; Kyoto University, Graduate School of Engineering Abe, Ryu; Kyoto University, Graduate School of Engineeing

ARTICLE

Mono-Transition-Metal-substituted Polyoxometalates as Shuttle Redox Mediator for Z-scheme Water Splitting under Visible Light

Received 00th January 20xx,
Accepted 00th January 20xx

DOI: 10.1039/x0xx00000x

Osamu Tomita, [a] Hiroki Naito, [a] Akinobu Nakada, [a] Masanobu Higashi [a] and Ryu Abe*[a b]

Because the majority of Z-scheme water splitting systems employ a shuttle redox mediator that allows electron transfer between two photocatalyst materials, the development of an effective redox mediator is crucial for improving the efficiency of Z-scheme systems toward the overall water splitting reaction. We recently revealed that some polyoxometalates (POMs) such as Manganese-substituted Keggin-type silicotungstate ($[SiW_{11}O_{39}Mn^{III/II}(H_2O)]^{5-/6-}$) can function as stable redox mediators. However, the limited number of POMs available for the Z-scheme system hinders the understanding of the fundamental properties of the employed POM. Herein, a series of Vanadium-substituted POMs, i.e., $[XV^{V}W_{11}O_{40}]^{n-}/[XV^{IV}W_{11}O_{40}]^{(n+1)-}$ (X = B, Si, and P), and a Cobalt-substituted POM $[SiW_{11}O_{39}Co^{III}(H_2O)]^{5-}/[SiW_{11}O_{39}Co^{II}(H_2O)]^{6-}$ were synthesized. Moreover, the fundamental properties, such as redox potential and chemical stability, of the POMs and their impact on water splitting photocatalysis efficiency was evaluated to provide guidance for designing efficient POM redox mediators. The substitution of constituent elements was found to affect their redox potentials, chemical stability under varied pH conditions, light absorption, and photocatalytic activity. All V-substituted POMs were found to possess an appropriate redox potential (i.e., between the potentials of water reduction and oxidation); however, their relatively high absorption in the visible light region appeared to be a disadvantage in terms of light shielding. Among the V-substituted ones, the $[SiV^{V}W_{11}O_{40}]^{5-}/[SiV^{IV}W_{11}O_{40}]^{6-}$ exhibited stability in repeated redox cycles over a wider pH range (2.5–6.5). In contrast, the redox potential of $[SiW_{11}O_{39}Co^{III}(H_2O)]^{5-}/[SiW_{11}O_{39}Co^{II}(H_2O)]^{6-}$ was more positive than the water oxidation potential, making it unsuitable for use as a redox mediator.

Introduction

Solar-light-induced water splitting using semiconductor photocatalysts has received considerable research attention because it facilitates the clean production of H_2 directly from water.[1–13] However, to achieve practically high solar-to-hydrogen efficiency, much more effective utilization of photons in the visible light region is indispensable. Z-scheme-type water splitting, mimicking the two-step photoexcitation mechanism of natural photosynthesis, has been proven to be a promising approach for harvesting visible light.[10,11,14–34] Typically, Z-scheme systems consist of two different particulate photocatalysts—one for H_2 evolution and the other for O_2 evolution—and a redox mediator that dissolves in aqueous solutions and facilitates electron transfer between the two photocatalysts. Thus, developing narrow-bandgap semiconductors for visible-light absorption and efficient redox mediators is crucial for improving their total efficiency toward Z-scheme water splitting. However, the choice of effective redox mediators has been limited to a few ion couples such as iodate/iodide (IO_3^-/I^-) and trivalent iron/divalent (Fe^{3+}/Fe^{2+}), along with some metal complexes such as $[Fe(CN)_6]^{3-/4-}$, $[Co(bpy)_3]^{3+/2+}$.[30–32] Although both IO_3^-/I^- and Fe^{3+}/Fe^{2+} have been proven to mediate electrons between various combinations of photocatalysts, their widespread application has been hindered by certain drawbacks. For example, the multi-electron redox nature of IO_3^-/I^- ($IO_3^- + 6H^+ + 6e^- \rightarrow I^- + 3H_2O$) often hampers surface reactions and, thus, lowers the total efficiency, despite the advantage that it can work under mild conditions of pH 5–9, whereat most photocatalysts do not undergo deactivation (e.g., dissolution). Although the one-electron redox nature of Fe^{3+}/Fe^{2+} generally allows fast redox reactions on photocatalyst surfaces in the absence of cocatalysts, the pH of aqueous solutions must be maintained below approximately 2.5 to avoid the precipitation of $Fe(OH)_3$, thus limiting the choice of semiconductor materials that are stable under such strongly acidic conditions. Furthermore, challenges such as the oxidative degradation of organic ligands impede the long-term use of metal complexes.

We recently revealed that some polyoxometalates (POMs), that is, Manganese-substituted Keggin-type silicotungstate ($[SiW_{11}O_{39}Mn^{III/II}(H_2O)]^{5-/6-}$) and its Molybdenum-substituted analog ($[SiMo^{VI/V}W_{11}O_{40}]^{4-/5-}$), can function as stable redox mediators for Z-scheme water

[a] Graduate School of Engineering, Kyoto University, Katsura, Nishikyo-ku, Kyoto 615-8510, Japan. E-mail: ryu-abe@scl.kyoto-u.ac.jp; Fax: +81 75383 2479; Tel: +81 75383 2479
[b] CREST, Japan Science and Technology Agency (JST), Kawaguchi, Saitama, 332-0012, Japan

†Electronic Supplementary Information (ESI) available: FT-IR spectra, Negative ion ESI mass spectra, cyclic voltammograms of polyoxometalate, and XP spectra of photocatalysts etc. See DOI: 10.1039/x0xx00000x

splitting.[33,34] Because their reversible redox behaviors are attributed to the valence change of the incorporated transition metals (Mn^{III}/Mn^{II} or Mo^{VI}/Mo^{V}), the appropriate substitution of cations will help tailor fundamental properties such as redox potential for efficient electron transfer between two photocatalytic materials. The relatively high stability over a wider range of pH is another advantage of POM materials, which facilitates its use as redox mediators. To provide guidance for designing efficient and useful POM redox mediators for Z-scheme systems, a more systematic investigation of the fundamental properties of POMs and the subsequent evaluation of their impact on the efficiency of each photocatalytic reaction are essential.

To this end, a series of Vanadium-substituted POMs with different central elements ($[BV^{V/IV}W_{11}O_{40}]^{6-/7-}$, $[SiV^{V/IV}W_{11}O_{40}]^{5-/6-}$, and $[PV^{V/IV}W_{11}O_{40}]^{4-/5-}$) and a Cobalt-substituted POM $[SiW_{11}O_{39}Co^{III/II}(H_2O)]^{5-/6-}$ were prepared and their fundamental properties such as chemical stability, redox potentials, and redox reversibility were evaluated under various pH conditions. In addition, Mn-substituted $[SiW_{11}O_{39}Mn^{III/II}(H_2O)]^{5-/6-}$, a previously reported POM for the Z-scheme,[33] was evaluated in detail for comparison with the present POMs. This particular POM was chosen for comparison because of its higher stability than that of Mo-substituted $[SiMo^{VI/V}W_{11}O_{40}]^{4-/5-}$, which was only stable at a limited pH of approximately 2.7.[34] Further the impact of their fundamental properties on the efficiency toward each photocatalytic reaction (half H_2 production or O_2 production) as well as overall Z-scheme water splitting was examined and discussed.

Results and discussion

Redox Potential and Stability of Transition-Metal-Substituted POMs

The redox potential of POMs is undoubtedly one of the determining factors in photocatalysis. In addition, chemical stability over a relatively wide pH range is required, because the progress of reactions over each photocatalyst leads to a local change in pH. Although all silicotungstates employed herein (Si*M* (*M* = V, Co, or Mn)) have previously been demonstrated to exhibit reversible redox cycles ascribed to the valence change of the incorporated cations,[35–37] their electrochemical analysis was carried out under various conditions (e.g., different solvents and supporting electrolytes). Thus, their redox behavior was evaluated in a fixed solution (i.e., phosphate buffer) herein.

Fig. 1-(a) shows the cyclic voltammograms of 1 mM Si*M* (*M* = V^{V}, Co^{II}, or Mn^{II}) dissolved in an aq. KH_2PO_4 solution (0.5 M, pH 4.4, purged with Ar gas) in the range of –0.2 +1.3 V (vs. Ag/AgCl). Based on the results in previous reports,[35,37–41] the pH of the aqueous electrolyte solution was first set at pH 4.4. Both SiV and SiCo exhibited one reversible peak, whereas the original unsubstituted one showed no peaks in this scan range (Fig. S1). Their redox potentials (i.e., half-wave potentials ($E_{1/2}$)) derived from the valence change of the incorporated $V^{V/IV}$ and $Co^{III/II}$ cations were determined to be +0.48 V and +1.03 V (vs. Ag/AgCl), respectively. In contrast, SiMn showed two reversible peaks, consistent with previous reports.[33,37] The observed values for Si*M* are in good agreement with those reported in previous studies (Fig. S2-(a) for SiV^{V}, and Fig. S2-(b) for $SiCo^{II}$), confirming the redox cycles of incorporated transition metals, namely, V^{V}/V^{IV}, Co^{III}/Co^{II}, Mn^{III}/Mn^{II}, and Mn^{IV}/Mn^{III}.[35,37,41]

Fig. 1-(b) shows the cyclic voltammetry (CV) profiles of V-substituted POMs consisting of different central elements *X*V (*X* = Si, P, or B). The $E_{1/2}$ values derived from V^{V}/V^{IV} cycles are +0.19 V, +0.48 V, and +0.62 V (vs. Ag/AgCl) for B, Si, and P, respectively. Appropriate pH values were selected for each experiment.

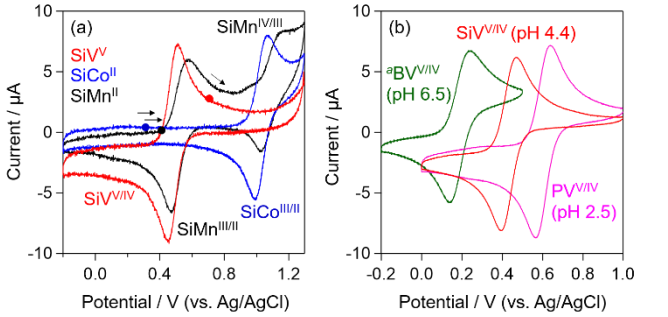

Fig. 1 Cyclic voltammograms of (a) Si*M* (*M* = V, Co, or Mn) in an aq. KH_2PO_4 solution (0.5 M, pH 4.4), and those of (b) *X*V (*X* = Si, P, or B) in aq. $K_xH_{3-x}PO_4$ solutions (^{a}0.05 M) (concentrations of Si*M* and *X*V: 1 mM; working electrode: GC, reference electrode: Ag/AgCl, counter electrode: Pt coil; scan rate: 50 mV s^{-1}).

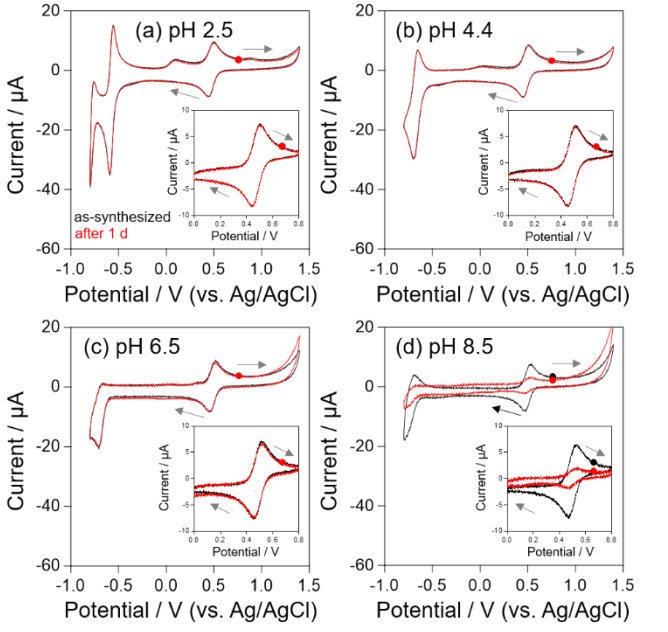

Fig. 2 Cyclic voltammograms of SiV (1 mM) in aq. $K_xH_{3-x}PO_4$ solutions (0.5 M) under different pH conditions after 1 day (scan rate: 50 mV s^{-1}).

As seen in Fig. 2, the CV shape of SiV remained unchanged even after being left for 1 d under pH conditions of 2.5–6.5. However, it changed significantly after 1 d at pH 8.5, indicating

the degradation or structural change of SiV. This evaluation indicated that the SiV is stable at pH values between 2.5 and 6.5, and unstable at pH values higher than 8.5. The stabilities of the other compounds were also investigated in an analogous manner (Figs. S3-6). The results are summarized in Fig. 3, in which the closed and open symbols indicate the stability-ensured and unstable regions, respectively.

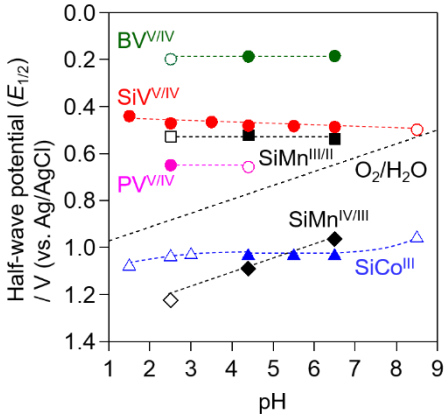

Fig. 3 Relationship between the half-wave potential ($E_{1/2}$ vs. Ag/AgCl) and the pH of the supporting electrolyte. (Open marks indicate the instability of POMs under the condition.)

For Si*M* (*M* = V, Co, or Mn), the $E_{1/2}$ values of SiV^{V}/SiV^{IV}, $SiCo^{III}/SiCo^{II}$, and $SiMn^{III}/SiMn^{II}$ were almost independent of pH, indicating that no H^+ was involved in these redox processes. In contrast, the $E_{1/2}$ values of $SiMn^{IV}/SiMn^{III}$ shifted with a change in pH, in accordance with the Nernst equation. These redox processes can be expressed by the following equations:

$$[SiV^{V}W_{11}O_{40}]^{5-} + e^- \longrightarrow [SiV^{IV}W_{11}O_{40}]^{6-}$$
$$E^0 = +0.69 \text{ V (vs. SHE at pH 4.4)}$$

$$[SiW_{11}O_{39}Co^{III}(H_2O)]^{5-} + e^- \longrightarrow [SiW_{11}O_{39}Co^{II}(H_2O)]^{6-}$$
$$E^0 = +1.24 \text{ V (vs. SHE at pH 4.4)}$$

$$[SiW_{11}O_{39}Mn^{III}(H_2O)]^{5-} + e^- \longrightarrow [SiW_{11}O_{39}Mn^{II}(H_2O)]^{6-}$$
$$E^0 = +0.72 \text{ V (vs. SHE at pH 4.4)}$$

$$[SiW_{11}O_{39}Mn^{IV}(OH)]^{5-} + e^- + H^+ \longrightarrow [SiW_{11}O_{39}Mn^{III}(H_2O)]^{5-}$$
$$E^0 = +0.40 \text{ V (vs. SHE at pH 6.5)}$$

The more positive potentials of $SiCo^{III}/SiCo^{II}$ and $SiMn^{IV}/SiMn^{III}$ than the water oxidation potential (indicated by the dotted line in Fig. 3) implies the possible occurrence of spontaneous water oxidation in the presence of these oxidized species.

As shown in Fig. 1-(b), the $E_{1/2}$ values of *X*V (*X* = P or B) are independent of pH, indicating that no H^+ is involved in the redox cycles, as previously reported,[38,40] which can be expressed as follows:

$$[PV^{V}W_{11}O_{40}]^{4-} + e^- \longrightarrow [PV^{IV}W_{11}O_{40}]^{5-}$$
$$E^0 = +0.83 \text{ V (vs. SHE at pH 2.5)}$$

$$[BV^{V}W_{11}O_{40}]^{6-} + e^- \longrightarrow [BV^{IV}W_{11}O_{40}]^{7-}$$

Electrochemical Oxidation and Reduction *via* Controlled Potential Electrolysis

The ability of each POM as an electron donor for H_2-evolution photocatalysis can be evaluated by using POM samples containing lower-valent cations, such as V^{IV}, Co^{II}, and Mn^{II}. On the other hand, samples with higher-valent cations (i.e., V^{V}, Co^{III}, and Mn^{III}) can be used as electron acceptors for O_2 evolution. A set of oxidized and reduced species is also essential for understanding other fundamental properties, such as optical absorption. Thus, the counterparts of the as-prepared samples were prepared *via* electrochemical oxidation or reduction *via* bulk electrolysis.

Fig. 4 shows an example of the results of such bulk electrolysis, the time course of the Coulomb number passed through the outer circuit during the reduction of SiV^{V} at a constant applied potential under an Ar atmosphere. The changes in the absorption spectra of the solution are shown inside the Fig. 4. The charge number was almost saturated at –9.83 C, nearly corresponding to the one-electron reduction of SiV^{V} (–9.65 C), and the spectral shape agrees well with those of SiV^{IV} as previously reported.[38] As for PV^{V} and BV^{IV}, Coulomb numbers and spectral changes were also saturated in bulk electrolysis at their corresponding appropriate pH values. In contrast, the Coulomb number during the electrochemical oxidation of $SiCo^{II}$ (at +1.18 V vs. Ag/AgCl at pH 4.4) exceeds the stoichiometric value (9.86 C), finally reaching 28.0 C at which no spectral change was observed (Fig. S7). This behavior suggests the simultaneous progress of water oxidation.

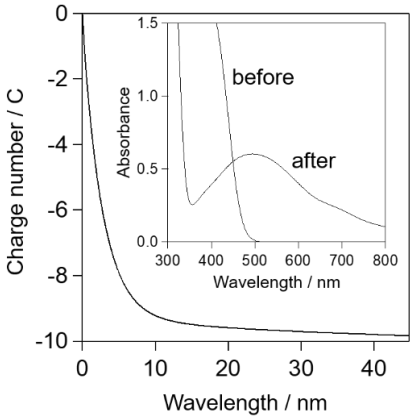

Fig. 4 Time course of the charge number passing through the outer circuit during the electrochemical reduction of SiV^{V} (2 mM) at +0.2 V (vs. Ag/AgCl) by controlled potential electrolysis in a bulk electrolysis cell (supporting electrolyte: 0.5 M of aq. KH_2PO_4 solution (50 mL, pH 4.4)). Inset: absorption spectra of the solution containing SiV before and after bulk electrolysis.

Fig. 5 (a) and (b) show the absorption spectra of oxidized and reduced species, respectively, prepared *via* bulk electrolysis. The unsubstituted one (SiW_{11}) shows typical absorption at wavelengths shorter than approximately 350 nm, attributed to the charge transfer in the W-O framework.[42] All V-substituted ones (*X*V^{IV}) exhibit absorption edges at a much

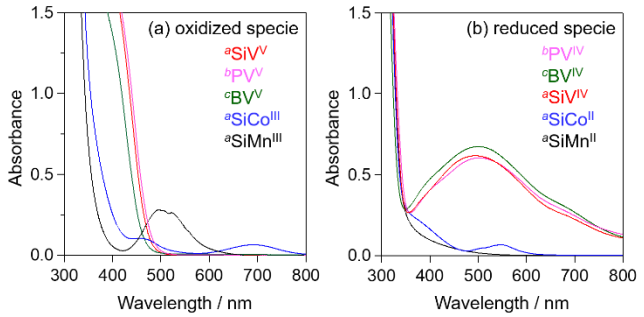

Fig. 5 Absorption spectra of solutions containing 1 mM of (a) oxidized species and (b) reduced species in aq. $^{a}KH_2PO_4$ solution (0.5 M, pH 4.4), aq. $^{b}K_xH_{3-x}PO_4$ solution (0.5 M, pH 2.5), and aq. $^{c}K_xH_{3-x}PO_4$ solution (0.05 M, pH 6.5). The spectrum of the unsubstituted one (SiW_{11}) is also shown for comparison.

longer wavelength of approximately 500 nm, attributed to the charge transfer from O to V. Such a shift was less obvious for $SiCo^{III}$ and $SiMn^{III}$, while additional absorption bands derived from the d-d transition of Co^{III} and Mn^{III} were observed at 692 and 495 nm, respectively. All the reduced species of XV^{IV} show a distinct and broad absorption peak at around 500 nm, which can be attributed to an intervalence charge transfer from V^{IV} to W^{VI}.[40] The strong absorption of *X*V POMs in both oxidized and reduced species in the visible light region will affect photocatalysis due to light shielding; this will be discussed in later sections. In contrast, $SiCo^{II}$ and $SiMn^{II}$ show much lower absorption in the visible light region.

As seen in Fig. 6-(a), the absorption of $SiCo^{III}$ prepared *via* bulk electrolysis spontaneously changed at pH 4.4, and finally became congruent with that of $SiCo^{II}$ after 15 h. This change is attributed to the spontaneous water oxidation by $SiCo^{III}$ ($4SiCo^{III} + 2H_2O \longrightarrow 4SiCo^{II} + O_2 + 4H^+$), as implied by the more positive potential of $SiCo^{III/II}$ than water oxidation potential. This spontaneous change was substantially suppressed by decreasing the pH, as shown in Fig. 6-(b), most probably due to the decreased driving force for electron transfer (see Fig. 3). Based on these results, the appropriate pH value for the photocatalytic evaluation of $SiCo^{III}/SiCo^{II}$ was set to 3.0.

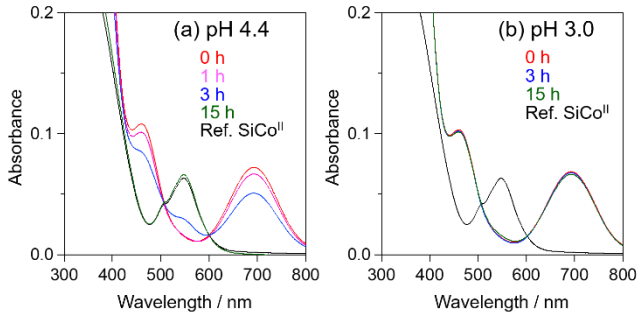

Fig. 6 UV-vis spectral change of solution containing $SiCo^{III}$ (1 mM) in (a) aq. KH_2PO_4 solution (0.5 M, pH 4.4), and (b) aq. $K_xH_{3-x}PO_4$ solution (0.5 M, pH 3.0) under dark conditions after bulk electrolysis, and the spectrum of $SiCo^{II}$ for comparison.

Photocatalytic H_2 Evolution Using POMs as an Electron Donor

The ability of POMs as an electron donor for H_2 evolution was evaluated using Ru/$SrTiO_3$:Rh, which is a typical and efficient H_2-evolution photocatalyst working under visible light.[24] The redox potential of Rh^{4+}/Rh^{3+} embedded in a $SrTiO_3$ host is still elusive but was roughly estimated to be about +2.2 V (vs. SHE) based on the photoabsorption due to transition from Rh^{3+} dopants to the conduction band.[43]

Fig. 7-(a) shows the time courses of H_2 evolution from the aqueous solution of Si*M*′ with a low-valent sample (*M*′ = V^{IV}, Co^{II}, or Mn^{II}) upon visible light irradiation. The pH was adjusted to 4.4, whereat all three POMs were stable (see Fig. 3). Note that slight but obvious H_2 evolution occurred even in the absence of POM, most probably due to the oxidation of residual organics on the photocatalyst. The rate of H_2 evolution with $SiCo^{II}$ is almost the same as that without POMs, indicating the inefficiency of $SiCo^{II}$ as an electron donor for Ru/$SrTiO_3$:Rh. The presence of SiV^{IV} drastically increased the H_2 evolution rate. The amount of H_2 reached approximately 50 μmol, which is the expected value from the initial amount of SiV^{IV}. Both the absorption spectra and CV of the solution filtered after the reaction were almost the same as those of SiV^{V} (Fig. S8).

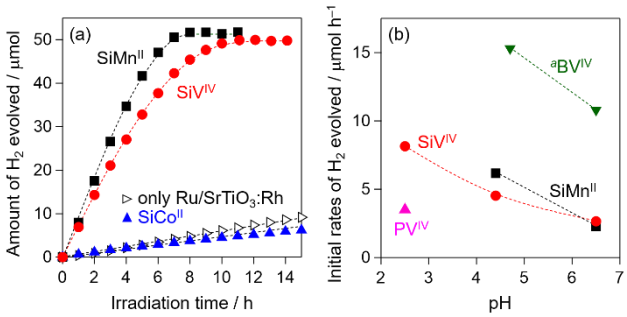

Fig. 7 (a) Time courses of H_2 evolution over Ru/$SrTiO_3$:Rh photocatalyst particles (0.1 g) suspended in an aq. KH_2PO_4 solution (0.5 M, 100 mL, pH 4.4) containing Si*M*′ (*M*′ = V^{IV}, Co^{II}, or Mn^{II}) (1 mM each) as an electron donor under visible light (λ > 400 nm) and the (b) initial H_2 evolution rate with each POM under various pH conditions in aq. $K_xH_{3-x}PO_4$ solutions (0.5 M, or ^{a}0.05 M for BV^{IV}, 100 mL) containing Si*M* (*M* = Co^{III}, V^{V}, or Mn^{III}) and XV^{IV}(*X* = P or B) (1 mM each).

These findings indicate the occurrence of stoichiometric photocatalysis as follows:

$$2H^+ + 2e^- \longrightarrow H_2 \text{ (–0.26 V vs. SHE at pH 4.4)}$$
$$SiV^{IV} + h^+ \longrightarrow SiV^{V} \text{ (+0.69 V vs. SHE at pH 4.4)}$$

The H_2 evolution rate gradually decreased before saturation was reached. Table S1 summarizes the influence of the initial concentration of SiV^{IV} and/or SiV^{V} on the H_2 evolution rate. The decreased concentration of SiV^{IV} from 1 to 0.5 mM slightly lowered the rate (from 6.9 to 5.3 μmol h^{-1}), whereas the co-presence of SiV^{V} (0.5 mM) with SiV^{IV} (1 mM) lowered it significantly (to 4.6 μmol h^{-1}). Thus, the major cause for the gradual decrease in the H_2 evolution rate is the occurrence of a backward reaction (i.e., reduction of SiV^{V} with photoexcited electrons). The lower rate of hole consumption might

contribute to it to some extent due to the decreased concentration of SiV^{IV}. The result for $SiMn^{II}$ was in good agreement with that of our previous report.[33]

Fig. 7-(b) shows the initial H_2 evolution rate for each POM at various pH values. The results of PV^{IV} and BV^{IV} were also included; the reaction with PV^{IV} was carried out only at pH 2.5 considering the results of the stability test (Fig. 3). The use of BV^{IV} resulted in significantly higher H_2 evolution rates than the others, while reactions were not carried out below pH 4 because of its insufficient stability. BV^{IV} showed superior ability as it had the most negative redox potential among XV^{IV}, providing the largest driving force for the oxidation on $SrTiO_3$:Rh. The sizable impact of the driving force on the H_2 evolution rate was also supported by the fact that SiV^{IV} and $SiMn^{II}$, which possess similar redox potentials, resulted in similar H_2 evolution rates. The rate of H_2 evolution with SiV^{IV} decreased monotonically with increasing pH. A similar tendency was observed for both BV^{IV} and $SiMn^{II}$. As shown in Fig. 3, the redox potentials of the POMs were pH-independent. In addition, the redox potential of Rh^{4+}/Rh^{3+} embedded in $SrTiO_3$ is assumed to be pH-independent, because it does not contain H^+ in the redox cycle. We found that the H_2 evolution rate on the Ru/$SrTiO_3$:Rh photocatalyst using methanol as a sacrificial electron donor also decreased monotonically with increasing pH (Fig. S9). Thus, the reduced H_2 evolution under higher pH conditions is a result of the decreased H^+ concentration dominantly, rather than the change in redox potentials.

Photocatalytic O_2 Evolution using POMs as an Electron Acceptor

The ability of POMs as electron acceptors for O_2 evolution was evaluated using WO_3, which is a well-known visible-light-responsive O_2-evolution photocatalyst.[5,6,44–47] Previous studies have shown that the typical conduction band minimum (CBM) and valence band maximum (VBM) of WO_3 are +0.41 and 3.18 V (vs. RHE), respectively.[48,49] The CBM and VBM are reported to shift negatively with increasing pH in accordance with the Nernst equation,[50] whereas the redox potentials of Si*M* (*M* = V and Mn) and *X*V (*X* = P, and B) are independent of pH, as shown in Fig. 3. The investigation of the activity of WO_3 under various pH conditions revealed that the O_2 evolution rate using a Ag^+ electron acceptor only slightly increased with increasing pH (Fig. S10), implying a negligible effect of pH on the intrinsic activity of O_2 generation, different from the H_2-evolution case.

Fig. 8-(a) shows the typical time courses of O_2 evolution from the solution containing each Si*M* (*M* = V^V, Co^{III}, or Mn^{III}). O_2 evolution was not observed from the solution containing only POMs (data not shown) or PtO_x/WO_3 under visible light. Given the spontaneous reduction of $SiCo^{III}$ to $SiCo^{II}$ at pH 4.4 (Fig. 6), the pH was set at 3.0 for $SiCo^{III}$. Although the stability of SiCo at pH 3.0, cannot be guaranteed for 1 d (see Fig. S3), it is expected to be stable for a much shorter time (~1.5 h) during the photocatalytic reaction. The presence of each POM triggered sizable O_2 evolution up to the almost stoichiometric amounts expected, while the rates depend on the amount of *M* incorporated. Among them, the use of $SiCo^{III}$ facilitated distinctly high O_2 evolution rate. This is undoubtedly due to the most positive redox potential of SiCo (+1.23 V vs. SHE at pH 3.0), which provides the largest driving force for electron transfer from the CBM (+0.23 vs. SHE at pH 3.0). The use of SiV^V resulted in a lower O_2 evolution rate compared to previous $SiMn^{III}$. The solutions after the reaction exhibited similar spectra and CV to the corresponding reduced species (Fig. S11-(a) and S12-(a)). Thus, the photocatalytic water oxidation proceeded almost stoichiometrically, accompanied by the reduction of POMs, as follows:

$2H_2O + 4h^+ \longrightarrow O_2 + 4H^+$
$SiCo^{III} + e^- \longrightarrow SiCo^{II}$ (+1.23 V vs. SHE at pH 3.0)
$SiV^V + e^- \longrightarrow SiV^{IV}$ (+0.69 V vs. SHE at pH 4.4)

Similar to H_2 evolution, the O_2 evolution rate of SiV^V gradually decreased before reaching saturation. As seen in Table S2, the rate was considerably lowered by the presence of SiV^{IV}, indicating the occurrence of a backward reaction (i.e., re-oxidation of SiV^{IV} by holes), while the decrease in SiV^{IV} possibly lowered it to some extent.

Fig. 8-(b) summarizes the initial O_2 evolution rate (closed symbols, left axis) and the difference between the redox potential and CBM of WO_3 with each POM (open symbols, right axis) under various pH conditions. Among them, SiV^V shows relatively high rates in a wide range of pH values. The O_2 evolution rate monotonically increased with the increase in pH. The enhanced O_2 evolution by pH increase was more significant for $SiMn^{III}$ compared to the case of SiV^V and BV^V.

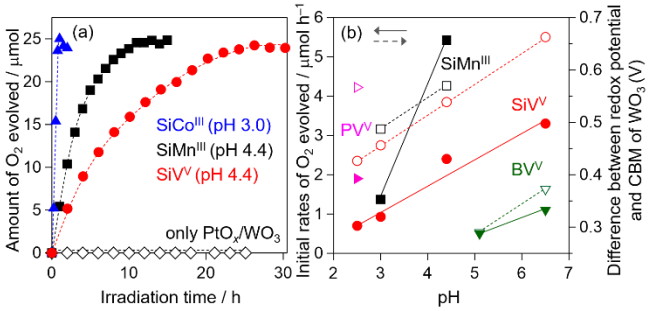

Fig. 8 (a) Time courses of O_2 evolution over PtO_x/WO_3 photocatalyst particles (0.1 g) suspended in an aq. KH_2PO_4 solution (0.5 M, 100 mL, pH 4.4) containing Si*M* (*M* = V^V, Co^{III}, or Mn^{III}) (1 mM each) as an electron acceptor under visible light (λ > 400 nm) and the (b) initial O_2 evolution rate with each POM under various pH conditions in aq. $K_xH_{3-x}PO_4$ solutions (0.5 M, or [a]0.05 M for BV^{IV}, 100 mL) containing Si*M* (*M* = Co^{III}, V^V, or Mn^{III}) and *X*V^{IV} (*X* = P or B) (1 mM each) (closed symbols, left axis), and the potential difference between the redox potential and CBM of WO_3 (open symbols, right axis).

It should be noted here that the light absorption of WO_3 overlapped well with those of SiV^V and BV^V (Fig. 9). Thus, the O_2 evolution rates are probably affected not only by the original electron accepting ability but also by the difference in photoabsorption (e.g., between SiV^V and $SiMn^{III}$). This complicates the discussion on the ability of POMs as a shuttle redox mediator with different substituted transition metals. Fortunately, three *X*V POMs (*X* = P, B, Si) exhibited similar photoabsorption properties (Fig. 5), facilitating discussion on

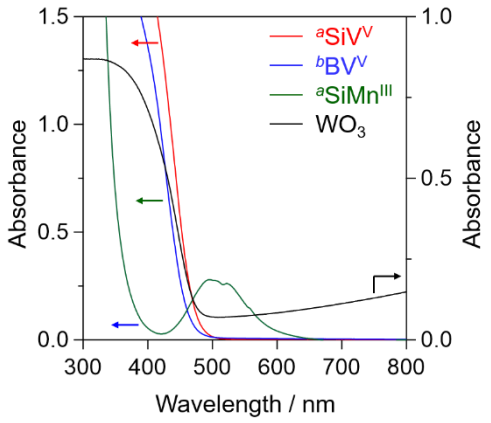

Fig. 9 Absorption spectra of solutions containing 1 mM of SiV^V, $SiMn^{III}$ in aq. $^aKH_2PO_4$ solution (0.5 M, pH 4.4), and BV^V in aq. $^bK_xH_{3-x}PO_4$ solution (0.05 M, pH 6.5) (left axis), and the absorption spectrum of the unmodified WO_3 sample.

the impact of redox potential on O_2 evolution independent of the light shielding effect. The notable correlation between the energy difference and the O_2 evolution rate (PV^V at pH 2.5, SiV^V at varied pH, and BV^V pH 6.5) strongly suggests that the driving force change by varying the pH has a significant effect on the O_2 evolution.

Z-scheme Water Splitting by Using POM as a Shuttle Redox Mediator

Finally, the Z-scheme water splitting system was constructed by combining an O_2-evolution photocatalyst and a H_2-evolution photocatalyst in the presence of each POM. Previous studies on Z-scheme systems with conventional redox systems such as IO_3^-/I^- have revealed the presence of an optimum concentration of the redox mediator for enhanced water splitting, in most cases providing volcano-type plots.[51] This is caused by the balance between the rates of H_2- and O_2-evolution photocatalysis; for example, a higher concentration of electron donors (i.e., I^-) can enhance H_2 evolution but at the same time lower the O_2 evolution due to the preferential oxidation of the donor to water.

Fig. 10 shows the gas evolution rates of reactions initiated with various initial concentrations of an oxidized sample (i.e., SiV^V or $SiMn^{III}$). All the examined cases led to simultaneous and stoichiometric generation of H_2 and O_2 (see some typical time courses in Fig. 11). For $SiMn^{III}$, a conventional volcano shape with a maximum efficiency of approximately 0.5 mM was obtained. The obtained optimum concentration (0.5 mM) is much lower than that of previously reported Z-scheme systems (e.g., typically 5 mM for IO_3^-/I^-, 2 mM for Fe^{3+}/Fe^{2+}). Surprisingly, in contrast with the results of half reactions (Figs. 7 and 8), the use of SiV^V afforded higher efficiency in water splitting over the entire range of redox concentrations; moreover, an unusual maximum different from the conventional volcano one can be found at approximately 0.1 mM. A possible explanation for this result is the difference in the photoabsorption properties of $SiMn^{III}$ and SiV^V, as shown in Fig. 9. The strong absorption of SiV^V at wavelengths shorter than 500 nm completely overlaps with the absorption of WO_3, while $SiMn^{III}$ exhibits much lower absorption in the range of 380–460 nm. The half reactions were initiated with relatively high concentrations (i.e., 1 mM) of POMs to ensure the accuracy of the molar amount of gas produced; such a high concentration of POM is undoubtedly disadvantageous for SiV^V, and thereby lowers the O_2 evolution rate. In contrast, we can initiate Z-scheme water splitting even with a much lower concentration of POMs, consequently disclosing the superior feature of SiV^V to the previous $SiMn^{III}$ as the shuttle redox mediator. Another probable reason is the considerable influence of the backward reaction on the O_2 evolution system. As revealed by the results shown in Table S2, O_2 evolution was significantly lowered by the co-presence of reduced SiV^{IV}, indicating the preferential occurrence of backward oxidation of SiV^{IV} by holes. In contrast, the coexistence of the H_2-evolution photocatalyst can lower the concentration of SiV^{IV} in a steady state by the prompt oxidation of SiV^{IV} on the H_2-evolution photocatalyst, consequently improving the O_2 evolution on WO_3. The ratio of SiV^{IV} and SiV^V in the steady state was confirmed to be approximately 3:7 in a typical Z-scheme reaction initiated with 0.5 mM of SiV^V.

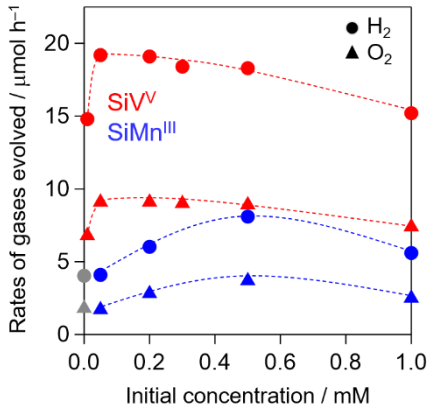

Fig. 10 Dependence of the rates of gases evolved on the pH of aq. KH_2PO_4 solutions (0.05 mM, 100 mL, pH 4.4) over PtO_x/WO_3 (0.3 g) and $Ru/SrTiO_3$:Rh (0.1 g) containing the oxidized specie SiV^V or $SiMn^{III}$ as a redox couple under visible light. The leftmost gray color symbols indicate the results in the absence of redox mediator.

Fig. 11 shows some typical time courses of gas evolution under visible light using a mixture of two photocatalysts, PtO_x/WO_3 (0.3 g) and $Ru/SrTiO_3$:Rh (0.1 g) containing (a) SiV^V and (b) $SiMn^{III}$. The amounts of H_2 and O_2 evolved after 10 h of irradiation exceeded the molar amount of SiV^V added to the solution (5 or 50 μmol). Based on the results for the reaction initiated with 0.05 mM of SiV^V (the total amount of O_2 evolved: approximately 80 μmol, the amount of SiV added: 5 μmol, Figure 11), for example, the TON in the redox cycle of $SiV^{V/IV}$ will be at least 64 by assuming that 4 electrons are required to evolve one O_2 molecule, indicating sufficient redox cycle of $SiV^{V/IV}$. The apparent quantum efficiency (AQE) of gases evolution over the mixture of PtO_x/WO_3 and $Ru/SrTiO_3$:Rh from the aq. solution containing SiV^V (0.05 mM) is determined to be approximately 1.6% at 405 nm. BV and PV were also

found to function stably as redox mediators at their respective appropriate pH values, generating H_2 and O_2 in a stoichiometric ratio (please see Fig. S13). SiV shows a higher gas evolution rate than the others, probably due to the balance of the driving force for the oxidation and reduction of each POM. As seen in Fig. S14, SiCo was unsuitable as a redox mediator owing to its more positive redox potential than the water oxidation potential, as expected from the results of H_2 evolution (Fig. 7). These results indicate that SiV has suitable properties as a redox couple among those examined in the present study. Moreover, the SiV couple has a disadvantage of photoabsorption overlapping with that of conventional photocatalysts; this can be mitigated by initiating a Z-scheme reaction with a significantly lower concentration, allowing the use of V-based POMs as a shuttle redox mediator.

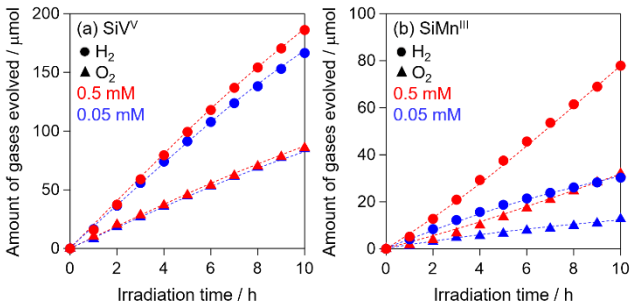

Fig. 11 Time courses of photocatalytic evolution of H_2 (circles) and O_2 (triangles) using a mixture of PtO_x/WO_3 (0.3 g) and $Ru/SrTiO_3$:Rh (0.1 g) suspended in an aq. KH_2PO_4 solution (0.05 M, 100 mL, pH 4.4) containing (a) SiV^V and (b) SiMn^{III} under visible light.

Conclusion

We demonstrated that V-substituted Keggin-type POMs can function as a redox mediator for a Z-scheme water splitting system under visible light. POMs, XV^V/XV^{IV}, where X = B^{3+}, Si^{4+}, or P^{5+}, and SiCo^{III}/SiCo^{II} were synthesized and applied to Z-scheme water splitting as a redox mediator. The redox cycle between XV^V and XV^{IV} was found to possess the applicable redox potential, and SiV^V was found to be chemically stable in a wide pH range (2.5–6.5) compared to others. Photocatalytic O_2 evolution using XV^V as an electron acceptor over PtO_x/WO_3 and H_2 evolution using XV^{IV} as an electron donor over $Ru/SrTiO_3$:Rh were demonstrated at appropriate pH values for each XV. SiCo^{III} was found to function as an electron acceptor; however, the ability of SiCo^{II} as an electron donor for $Ru/SrTiO_3$:Rh is insufficient because of its positive potential. Although SiV has relatively strong light absorption in the visible light range, which is considered to be a disadvantage for this reaction, it showed a higher gas evolution rate in Z-scheme overall water splitting than SiMn, which has a similar redox potential. The obtained results indicate the more suitable electron transfer characteristics of SiV as a redox couple. Furthermore, these results show the promising potential of POMs as a shuttle redox mediator for constructing more efficient and stable Z-scheme water splitting systems. The introduction of multiple transition metals, such as vanadium species, into frameworks will also broaden the application of POMs.

Experimental

All reagents were commercially available and used without further purification (please see the ESI for detailed information). Potassium salts of Keggin-type POMs, $K_8[SiW_{11}O_{39}]\cdot nH_2O$,[52] $K_5[SiVW_{11}O_{40}]\cdot nH_2O$,[36] $K_6[SiW_{11}O_{39}Co(H_2O)]\cdot nH_2O$,[35] $K_6[SiW_{11}O_{39}Mn(H_2O)\cdot nH_2O$,[37] $K_4[PVW_{11}O_{40}]\cdot nH_2O$,[53] and $K_7[BVW_{11}O_{40}]\cdot nH_2O$[40] were prepared according to previously reported methods. The preparation procedures for $K_8[SiW_{11}O_{39}]\cdot nH_2O$ and $K_5[SiVW_{11}O_{40}]\cdot nH_2O$ are shown below as representatives (those of others are shown in the ESI).

Preparation of Lacunary POM $K_8[SiW_{11}O_{39}]\cdot nH_2O$

A potassium salt of undecatungstosilicate tridecahydrate ($K_8[SiW_{11}O_{39}]\cdot nH_2O$) was prepared according to a previously reported method.[52] A total of 110 mmol of $Na_2WO_4\cdot 2H_2O$ was dissolved in Milli-Q water (300 mL) and boiled under continuous stirring using a magnetic stirrer. Subsequently, 33 mL of HCl (4 M) was added to the solution dropwise over 40 min with continuous stirring using a magnetic stirrer, maintaining the temperature of the solution under boiling. Another aqueous solution was prepared by dissolving 10 mmol of $Na_2SiO_3\cdot 9H_2O$ (100 mL) and then added to the above solution just below the boiling temperature with continuous stirring. The mixed solution was further acidified by adding 10 mL of HCl (4 M), and then stirred for 1 h before being allowed to cool to room temperature and was then kept for 20 h. KCl (30 g) was added to the solution to generate a white precipitate. The white precipitate was filtered and thoroughly washed with 20 mL of KCl (1 M) solution and 10 mL of Milli-Q water sequentially, and finally dried in air. Hereafter, the obtained samples are denoted as SiW_{11}. The hydration number in the obtained sample was determined to be 11 based on the sample weight measured by thermogravimetry (TG). Anal. Calc. for $K_8[SiW_{11}O_{39}]\cdot 11H_2O$, K: 9.8, Si: 0.9, W: 63.5 wt.%., Found, K: 8.5, Si: 0.8, W: 66.0 wt.%.; H_2O: 7.1 wt.%

Preparation of V-substituted Silicotungstate $K_5[SiVW_{11}O_{39}O]\cdot nH_2O$

A V-substituted Keggin-type silicotungstate *n*-hydrate ($K_5[SiVW_{11}O_{40}]\cdot nH_2O$) was prepared from SiW_{11} according to a previously reported method.[36] A total of 3.3 mmol of $NaVO_3$ was dissolved in 6.6 mL of Milli-Q water. Subsequently, 26 mL of HCl (1 M) was added to the solution under continuous stirring, and then 2.2 mmol of $K_8[SiW_{11}O_{39}]\cdot 11H_2O$ was added. After the solution was stirred for 15 min, 5 g of KCl was added to the solution, which generated a yellow precipitate. The precipitate was filtered and recrystallized from boiling water (5 mL) to afford $K_5[SiVW_{11}O_{40}]\cdot 11H_2O$ (hereafter denoted as SiV^V). The hydration number determined using the TG was 11. Anal. Calc. for $K_5[SiVW_{11}O_{40}]\cdot 11H_2O$, K: 6.2, Si: 0.9, V: 1.6, W: 64.5 wt.%. Found, K: 6.4, Si: 0.8, V: 1.8, W: 65.8 wt.%; H_2O: 7.5 wt.%

Characterization of POMs

The infrared (IR) spectrum of SiW_{11} was measured using an FT-IR spectrometer (FT-IR 4200, JASCO) with a KBr pellet (see Fig. S15). The redox behavior of the prepared POMs was investigated by CV. The electrochemical cell consisted of a glassy carbon (GC) working electrode (inner diameter: 3 mm, BAS Inc.), a saturated Ag/AgCl reference electrode (saturated KCl, +0.198 V vs. SHE at 25 °C), and a Pt coil counter electrode. Before measurements, the GC electrode was polished using diamond slurry (1 μm, BAS Inc.) and alumina slurry (0.05 μm, BAS Inc.) sequentially, and washed with Milli-Q water. Before the measurements, each electrolyte solution was thoroughly purged with Ar gas (99.9%) to remove the dissolved air. The potential of the GC electrode was controlled using a potentiostat (VersaSTAT 3, Princeton Applied Research). The cyclic voltammograms of the prepared POMs were measured in the supporting electrolyte solution used in previous reports (Fig. S2 and S3), aq. KH_2PO_4 buffer (0.5 M, pH 4.5) for SiW_{11},[37] aq. CH_3COOH/CH_3COONa buffer solution (0.5 M, pH 4.5) for SiV,[41] aq. CH_3COOH/CH_3COONa (0.1 M) + $NaClO_4$ (0.9 M) buffer solution (pH 4.7) for SiCo,[54] aq. KH_2PO_4 buffer (0.5 M, pH 4.5) for SiMn,[37] aq. H_2SO_4 solution (0.1 M, pH 1.2) for PV,[40] and aq. $Na_xH_{3-x}PO_4$ buffer solution (0.1 M, pH 6.0) for BV.[40] The absorption spectra of the solutions containing each POM were measured using a UV-vis. spectrometer (UV-1800, Shimadzu). The molecular weights of the POMs were determined using ESI-MS (MS: Exactive, HPLC: Accela 600 series, Thermo Fisher Scientific) (see Figs. S16-19). An inductively coupled plasma spectrometer (iCAP 7000 Duo, Thermo Fisher Scientific) was used for the elemental analysis. The water content was determined by ignition loss at 300 °C using a thermogravimetric analyzer (Thermo plus EVO2, Rigaku). The Brunauer-Emmett-Teller (BET) surface area of the photocatalyst sample was measured (BELSORP-mini II, MicrotracBEL Corp.). The valence state of the Pt species on WO_3 was investigated through X-ray photoelectron spectroscopy (XPS, MT-5500, ULVAC-PHI, Inc., Mg Kα). To correct the chemical shift of the other elements, the binding energy of the C1s peak was adjusted to 284.6 eV.

Controlled Potential Electrolysis of POMs

POMs incorporated with low-valent transition metals ($[SiVW_{11}O_{40}]^{6-}$ and $[PVW_{11}O_{40}]^{5-}$, denoted as SiV^{IV} and PV^{IV}, respectively) and those incorporated with high-valent transition metals ($[BVW_{11}O_{40}]^{6-}$ and $[SiW_{11}O_{39}Co(H_2O)]^{5-}$, denoted as BV^{V} and $SiCo^{III}$) were obtained by controlled potential electrolysis in a bulk electrolysis cell consisting of a porous carbon working electrode (BAS Inc.), Ag/AgCl reference electrode, and Pt counter electrode. The solutions containing the required amount of POMs were purged with Ar gas to remove dissolved air before the electrolysis, and the potentials of the working electrode determined from the CV results at +0.20 V (vs. Ag/AgCl) for SiV^{V} or PV^{V}, +1.18 V for $SiCo^{II}$ and +0.50 V for BV^{IV} were applied using a potentiostat in the aq. $K_xH_{3-x}PO_4$ solution. The bulk electrolysis was continued until the total Coulomb number reached the stoichiometric values calculated from the initial amount of each POM added, and/or no further spectral changes in the absorption spectra were observed.

Preparation of Photocatalyst Particles

WO_3 samples loaded with Pt species as cocatalysts were prepared using an impregnation method and subsequent calcination at 550 °C in air (Pt precursor: $H_2PtCl_6{\cdot}6H_2O$, amount of Pt species: 0.5 wt.% as metal calculated relative to the amount of photocatalyst particles) and used as an O_2-evolution photocatalyst (detailed preparation procedure is shown in the ESI).[33,34,45] The XP spectra shown in Fig. S20 confirmed the presence of Pt^{II} species (e.g. PtO) at 550 °C in these samples., The samples are denoted as PtO_x/WO_3. The particles of strontium titanate doped with Rh species were prepared by a solid-state reaction, and the ruthenium species were loaded onto the obtained samples *via* the photodeposition method using $RuCl_3{\cdot}nH_2O$ as the Ru precursor (0.7 wt.% as metal) according to previous reports.[20] The samples will be denoted as $Ru/SrTiO_3$:Rh hereafter.

Photocatalytic Reaction Condition

The photocatalytic reaction was conducted using a top-irradiation-type Pyrex reaction cell connected to a closed gas circulation system. For photocatalytic O_2 evolution, 0.1 g of O_2-evolution photocatalyst was suspended using a magnetic stirrer in the $K_xH_{3-x}PO_4$ buffer solution (0.5 or 0.05 M, or 100 mL) containing the required amount of oxidized species of POMs (XV^{V} (*X* = Si, P, or B), $SiCo^{III}$, or $SiMn^{III}$) as an electron acceptor. The initial concentration of each POM was set to 1 mM (100 μmol), unless otherwise stated. For photocatalytic H_2 evolution, 0.1 g of $Ru/SrTiO_3$:Rh photocatalyst particles as an H_2-evolution photocatalyst was suspended in the $K_xH_{3-x}PO_4$ buffer solution and irradiated for 1 h before the reactions to remove residual organic compounds. The suspension was then added to the required amount of reduced species of POMs (XV^{IV} (*X* = Si, P, or B), $SiCo^{II}$, or $SiMn^{II}$) as an electron donor (1 mM unless stated). For the two-step water splitting reaction, $Ru/SrTiO_3$:Rh (0.1 g) suspended in the $K_xH_{3-x}PO_4$ buffer solution (0.05 M) in the side irradiation reaction cell was irradiated (λ > 400 nm) before the reaction. Then, PtO_x/WO_3 particles (0.3 g) and 50 μmol of each POM were added. The suspension (100 mL) in the reaction cell was finally exposed to visible light irradiation (λ > 400 nm) from a Xe lamp equipped with a cut-off filter and cold mirror. The temperature of the solution was maintained at 15 °C using a flow of external circulating cooling water during the reaction. The evolved gases were analyzed using an on-line gas chromatograph (GC-8A, Shimadzu, column: MS-5A, Ar carrier). After each photocatalytic reaction, the suspension was centrifuged, and the CV of the supernatant was measured under the same conditions as described above. The sample aliquots were also taken from the supernatant, and UV-vis absorption spectra were measured.

The apparent quantum efficiency (AQE) for the Z-scheme water splitting in the presence of SiV^{5+}/SiV^{4+} were measured by using a similar experimental arrangement. LED (λ = 405 nm, CL-1501, ASAHI Spectra CO., LTD.) was used as the light source. The photon flux of the monochromatic light was measured by

a silicon photodiode (Hioki 3664 optical power meter, Hioki E.E. Corporation). The AQE was calculated using the following equation:

$$AQE\ (\%) = 100 \times A \times R / I$$

where A is the number of photons required to generate one molecule of products (i.e., 8 for O_2 and 4 for H_2), R is the rate of gas evolution, and I is the number of incident photons (37 mW cm^{-2}).

Author Contributions

All authors revised the manuscript, approved the manuscript to be published, and agreed to be accountable for all aspects of the work in ensuring that questions related to the accuracy or integrity of any part of the work are appropriately investigated and resolved.

O. T.: Conceptualization, Investigation, Methodology, Resources, Visualization, Writing - original draft, Writing - review & editing. H. N.: Investigation, Visualization, Writing - original draft, Writing - review & editing. A. N.: Writing - review & editing. M. H.: Writing - review & editing. R. A.: Writing - original draft, Writing - review & editing, Supervision, Funding acquisition, Project administration.

Conflicts of interest

There are no conflicts to declare.

Acknowledgements

This work was financially supported by the JSPS KAKENHI Grant Number 17H06439 in Scientific Research on Innovative Areas "Innovations for Light-Energy Conversion (I4LEC) ", the Core Research for Evolutional Science and Technology (CREST) from the Japan Science and Technology Agency (JST), JSPS Core-to-Core Program, and Grant-in-Aid for Early-Career Scientists (20K15380). The authors are indebted to the technical division of Institute for Catalysis, Hokkaido University for their help in building the experimental equipment.

Notes and references

1 K. Domen, S. Naito, M. Soma, T. Onishi and K. Tamaru, *J. Chem. Soc. Chem. Commun.*, 1980, 543–544.
2 K. Domen, S. Naito, T. Onishi and K. Tamaru, *Chem. Phys. Lett.*, 1982, **92**, 433–434.
3 A. Kudo, A. Tanaka, K. Domen, K. Maruya, K. Aika and T. Onishi, *J. Catal.*, 1988, **111**, 67–76.
4 R. Abe, K. Shinohara, A. Tanaka, M. Hara, J. N. Kondo and K. Domen, *Chem. Mater.*, 1997, **9**, 2179–2184.
5 K. Sayama, R. Yoshida, H. Kusama, K. Okabe, Y. Abe and H. Arakawa, *Chem. Phys. Lett.*, 1997, **277**, 387–391.
6 T. Ohno, F. Tanigawa, K. Fujihara, S. Izumi and M. Matsumura, *J. Photochem. Photobiol. A Chem.*, 1998, **118**, 41–44.
7 G. Hitoki, T. Takata, J.N. Kondo, M. Hara, H. Kobayashi and K. Domen, *Chem. Commun.*, 2002, 1698–1699.
8 K. Maeda and K. Domen, *J. Phys. Chem. C*, 2007, **111**, 7851–7861.
9 Y. Lee, H. Terashima, Y. Shimodaira, K. Teramura, M. Hara, H. Kobayashi, K. Domen and M. Yashima,. *J. Phys. Chem. C*, 2007, **111**, 1042–1048.
10 K. Maeda and K. Domen, *J. Phys. Chem. Lett.*, 2010, **1**, 2655–2661.
11 F. E. Osterloh, *Chem. Mater.*, 2008, **20**, 35–54.
12 H. Lyu, T. Hisatomi, Y. Goto, M. Yoshida, T. Higashi, M. Katayama, T. Takata, T. Minegishi, H. Nishiyama, T. Yamada, Y. Sakata, K. Asakura and K. Domen, *Chem Sci.*, 2019, **10**, 3196–3201.
13 Q. Wang, M. Nakabayashi, T. Hisatomi, S. Sun, S. Akiyama, Z. Wangm, Z. Pan, X. Xiao, T. Watanabe, T. Yamada, N. Shibata, T. Takata and K. Domen, *Nat Mater.*, 2019, **18**, 827–832.
14 R. Abe, K. Sayama, K. Domen and H. Arakawa, *Chem. Phys. Lett.*, 2001, **344**, 339–344.
15 K. Sayama, K. Mukasa, R. Abe, Y. Abe and H. Arakawa, *Chem. Commun.*, 2001, **1**, 2416–2417.
16 H. Kato, M. Hori, R. Konta, Y. Shimodaira and A. Kudo, *Chem. Lett.*, 2004, **33**, 1348–1349.
17 R. Abe, T. Takata, H. Sugihara and K. Domen, *Chem. Commun.*, 2005, 3829–3831.
18 R. Abe, T. Takata, H. Sugihara and K. Domen, *Chem. Lett.*, 2005, **34**, 1162–1163.
19 R. Abe, K. Sayama and H. Sugihara, *J. Phys. Chem. B*, 2005, **109**, 16052–16061.
20 Y. Sasaki, A. Iwase, H. Kato and A. Kudo, *J. Catal.*, 2008, **259**, 133–137.
21 A. Kudo and Y. Miseki, *Chem. Soc. Rev.*, 2009, **38**, 253–278.
22 R. Abe, *J. Photochem. Photobiol. C Photochem. Rev.*, 2010, **11**, 179–209.
23 R. Abe, K. Shinmei, N. Koumura, K. Hara and B. Ohtani, *J. Am. Chem. Soc.*, 2013, **135**, 16872–16884.
24 R. Niishiro, S. Tanaka and A. Kudo, *Appl. Catal. B Environ.*, 2014, **150–151**, 187–196.
25 T. Kato, Y. Hakari, S. Ikeda, Q. Jia, A. Iwase and A. Kudo, *J. Phys. Chem. Lett.*, 2015, **6**, 1042–1047.
26 Y. Miseki, S. Fujiyoshi, T. Gunji and K. Sayama, *J. Phys. Chem. C*, 2017, **121**, 9691–9697.
27 A. Nakada, S. Nishioka, J. J. M. Vequizo, K. Muraoka, T. Kanazawa, A. Yamakata, S. Nozawa, H. Kumagai, S. I. Adachi, O. Ishitani and K. Maeda, *J. Mater. Chem. A*, 2017, **5**, 11710–11719.
28 H. Fujito, H. Kunioku, D. Kato, H. Suzuki, M. Higashi, H. Kageyama and R. Abe, *J. Am. Chem. Soc.*, 2016, **138**, 2082–2085.
29 Y. Wang, H. Suzuki, J. Xie, O. Tomita, D. J. Martin, M. Higashi, D. Kong, R. Abe and J. Tang, *Chem. Rev.*, 2018, **118**, 5201–5241.
30 W. Y. Wang, J. Chen, C. Li and W. M. Tian, *Nat. Commun.*, 2014, **5**, 4647
31 T. Shirakawa, M. Higashi, O. Tomita and R. Abe, *Sustainable Energy & Fuels*, 2017, **1**, 1065–1073.
32 Y. Sasaki, H. Kato and A. Kudo, *J. Am. Chem. Soc.*, 2013, **135**, 5441–5449.

33 K. Tsuji, O. Tomita, M. Higashi and R. Abe, *ChemSusChem*, 2016, **9**, 2201–2208.
34 Y. Iwase, O. Tomita, H. Naito, M. Higashi and R. Abe, *J. Photochem. Photobiol. A Chem.*, 2018, **356**, 347–354.
35 T. J. R. Weakley and S. A. Malik, *J. Inorg. Nucl. Chem.*, 1967, **29**, 2935–2944.
36 G. Hervé, A. Tézé and M. Leyrie, *J. Coord. Chem.*, 1979, **9**, 245–249.
37 M. Sadakane and E. Steckhan, *J. Mol. Catal. A Chem.*, 1996, **114**, 221–228.
38 D. P. Smith and M. T. Pope, *Inorg. Chem.*, 1973, **12**, 331–336.
39 A. Böhm, *Quantum Mech.*, 1979, **12**, 218–236.
40 J. J. Altenau, M. T. Pope, R. A. Prados and H. So, *Inorg. Chem.*, 1975, **14**, 417–421.
41 C. Li, Y. Zhang, K. P. O'Halloran, J. Zhang and H. Ma, *J. Appl. Electrochem.*, 2009, **39**, 421–427.
42 J. M. Fruchart, G. Herve, J. P. Launay and R. Massart, *J. Inorg. Nucl. Chem.*, 1976, **38**, 1627–1634.
43 R. Konta, T. Ishii, H. Kato and A. Kudo, *J. Phys. Chem. B*, 2004, **108**, 8992–8995.
44 J. R. Darwent and A. Mills, *J. Chem. Soc. Faraday Trans. 2 Mol. Chem. Phys.*, 1982, **78**, 359–367.
45 R. Abe, M. Higashi and K. Domen, *ChemSusChem*, 2011, **4**, 228–237.
46 K. Maeda, M. Higashi, D. Lu, R. Abe and K. Domen, *J. Am. Chem. Soc.*, 2010, **132**, 5858–5868.
47 O. Tomita, S. Nitta, Y. Matsuta, S. Hosokawa, M. Higashi and R. Abe, *Chem. Lett.*, 2017, **46**, 221–224.
48 Y. Ping and G. Galli, *J. Phys. Chem. C*, 2014, **118**, 6019–6028.
49 S. Corby, L. Francàs, S. Selim, M. Sachs, C. Blackman, A. Kafizas and J. R. Durrant, *J. Am. Chem. Soc.*, 2018, **140**, 16168–16177.
50 P. K. Shen and A. C. C. Tseung, *J. Mater. Chem.*, 1992, **2**, 1141–1147.
51 R. Abe, *Bull Chem. Soc. Jpn.*, 2011, **84**, 1000–1030.
52 A. Tézé and G. Hervé, *Inorg. Synth.*, 1990, **27**, 85–96.
53 P. J. Domaille, *J. Am. Chem. Soc.*, 1984, **106**, 7677–7687.
54 J. L. Samonte and M. T. Pope, *Can. J. Chem.*, 2001, **79**, 802–808.